Perturbative QCD calculation of real and virtual Compton scattering

Glennys R. Farrar and Huayi Zhang
Department of Physics and Astronomy, Rutgers University, Piscataway, New Jersey 08855
(Received 29 September 1989)

We present the predictions of perturbative QCD for Compton scattering as a function of photon virtuality. Individual helicity amplitudes are given, along with formulas to permit calculation of the $eN \to e'N'\gamma$ amplitudes. We discover remarkable structure in some of the amplitudes as a function of photon virtuality. Since $eN \to e'N'\gamma$ contains a contribution from Bethe-Heitler scattering, whose magnitude and phase are known, the phases of the virtual Compton amplitudes can in principle be measured by interference with it. It has been shown that the leading-twist behavior of high-energy, large-angle Compton scattering is not affected by soft physics; thus at sufficiently high energies these predictions provide a stringent test of QCD.

I. INTRODUCTION

In collaboration with Sterman, we have recently demonstrated[1] that the energy and angular dependence, magnitude, and phase of Compton scattering are reliable asymptotic predictions of perturbative QCD (PQCD), unaffected by soft physics. As a result, prediction of the virtual Compton (VC) scattering amplitudes, and elaboration and verification of existing results[2,3] for the real Compton scattering amplitudes, have become important goals. Virtual Compton scattering is of special interest, as compared to real Compton scattering, for two reasons. First, the photon virtuality provides an additional dimensional variable so that predictions in this case are for a function of two rather than one variable: q^2/s as well as t/s. Furthermore, due to the interference of Bethe-Heitler scattering with the VC contribution to $eN \to e'N'\gamma$ illustrated in Fig. 1, phase information on the VC amplitudes can be obtained more easily than in the real Compton case. Thus virtual Compton scattering is a demanding testing ground for PQCD and, as we show below, a sensitive probe of the nucleon wave function.

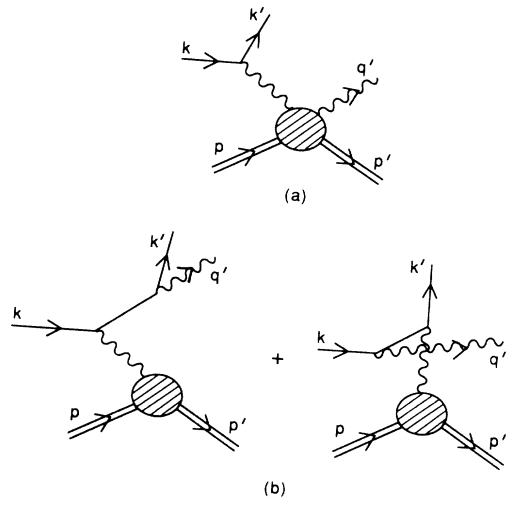

FIG. 1. (a) Virtual Compton and (b) Bethe-Heitler contributions to $eN \to eN'\gamma$.

We find truly remarkable predictions for the behavior of certain helicity amplitudes, reflecting subtle coherent effects in the perturbation theory. These will be most interesting to investigate experimentally. They also suggest that the experimentally observed structure in the spin dependence of pp elastic scattering may not be in conflict with PQCD, as is widely supposed.

Except for technical complications in the algebraic Feynman-diagram calculation coming from the nonvanishing virtuality of the photons, and the fact that the formulas for the amplitudes are considerably longer in the virtual case, which makes the numerical integrations over the hadron wave functions more time consuming, the calculations are very similar in the real and virtual cases. In this paper we present the details of our techniques, and the helicity amplitudes for the real and virtual Compton scattering processes $\gamma p \to \gamma p$, $\gamma p \to \gamma \Delta^+$, $\gamma n \to \gamma n$, $\gamma n \to \gamma \Delta^0$, and $\gamma \Delta^+ \to \gamma \Delta^+$. The latter reaction yields insight into the physics of $\gamma p \to \gamma p$ and $\gamma p \to \gamma \Delta^+$ and may be of interest in experiments on nuclear targets. Where our results overlap those of Refs. 2 and 3 we find the numerical-integration results of the previous work to have been inaccurate. We will supply a computer file with our algebraic formulas for the Compton amplitudes to persons requesting it, as they are too lengthy to give here.

II. TECHNIQUES

The algebraic techniques and algorithms which form the basis of our computer program DIAG, with which we have obtained the Feynman amplitudes for the quark-level scattering, will be described elsewhere. Using it, we have reproduced known results for the meson and baryon form factors, and for $\gamma\gamma \to MM'$ and $\gamma\gamma \to B\bar{B}'$, and have evaluated the amplitudes for meson-meson and meson-baryon scattering. In short, the program which we have used to produce the virtual and real Compton amplitudes has been verified to work in a large variety of cases. Some of the features arising when one photon is virtual already occur in the form-factor calculations.

Moreover when both photons are real the amplitudes are related by crossing symmetry to the $\gamma\gamma \to B\bar{B}'$ amplitudes, where our results agree with those of two independent previous calculations.[45] Our algebraic formulas in the $q^2 \to 0$ limit agree with those obtained by Maina[2,3] for real Compton using the program written by him and Neri. We have checked that our expressions behave properly in the $q^2 \to 0$ limit: amplitudes involving temporal and longitudinal photon polarizations vanish, and $A_{LR}(\theta) = A_{RL}(\pi - \theta)$, where, e.g., A_{LR} refers to a helicity amplitude for left (right) circularly polarized initial (final) photons. Finally, we have checked the gauge invariance of our formulas under both U(1) and SU(3) gauge transformations. For the above reasons we are satisfied as to the correctness of the algebraic expressions we use for the quark-level scattering amplitudes.

The quark-level scattering amplitudes, which depend on scattering angle, q^2/s, and the momentum fractions of the quarks, must be integrated over the wave functions of the initial and final baryons, describing how the quarks share the hadrons' momenta. This integration contains integrable singularities corresponding to the kinematic possibility that the scattering takes place as a sequence of on-shell scatterings. Although it was shown in Ref. 1 that the singularity does not destroy the light-cone dominance of Compton scattering, it nevertheless makes the numerical integration difficult. Our approach has been to simply keep the $i\epsilon$'s which belong in the propagators, so that the integrand is explicitly complex, and evaluate the result for a series of ϵ's. We find that it converges nicely, as illustrated in Figs. 2 and 3 for one helicity configuration. Although the convergence is better in some cases than others, in all cases it is excellent by the time ϵ is as small as 0.01. When ϵ is less than ~ 0.005 the functions are so singular that they cannot be integrated accurately in a reasonable amount of computer time, which accounts for the waviness of the curves for very small ϵ; this contains no physics. Unless explicitly stated otherwise, results presented below are for $\epsilon = 0.005$. The numerical integration required to complete the work reported in this paper consumed ~ 100 hours of Cyber 205 time at the John von Neumann Computer Center.

Maina[2] took a more subtle approach, and Taylor expanded the numerators of the singularities in a symmetrical region about the singularity, so that the singular part could be set to zero. We extensively investigated this procedure, using his programs (because our final predictions differ significantly from those of Ref. 3), and discovered, somewhat surprisingly, that the numerical accuracy of a Monte Carlo integration of his regulated amplitudes is actually much worse than either (a) what is indicated by the error estimate of his integration routine (VEGAS), or (b) that of our "brute-force" regulation method. It turns out that his regulation procedure, while eliminating the singularity itself, does not result in a sufficiently smooth function where the singularities approach the edge of the integration domain. Since our algebraic expressions agree with his, our numerical results are well behaved, and we have identified a source of numerical inaccuracy in his procedure, we believe that the results presented here are the correct ones.

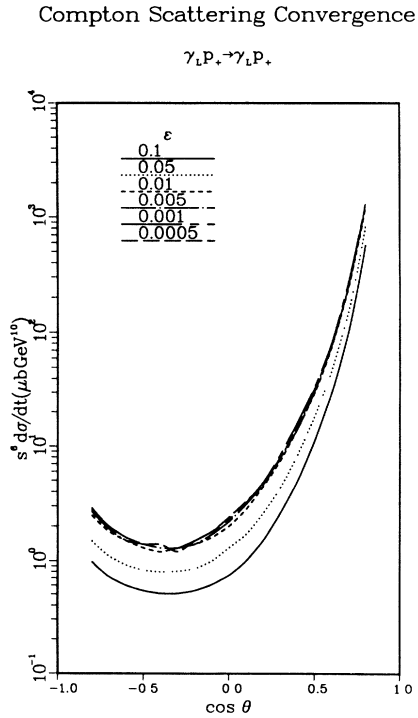

FIG. 2. Predictions for the cross section of $\gamma_L p_+ \to \gamma_L p_+$, for various choices of ϵ.

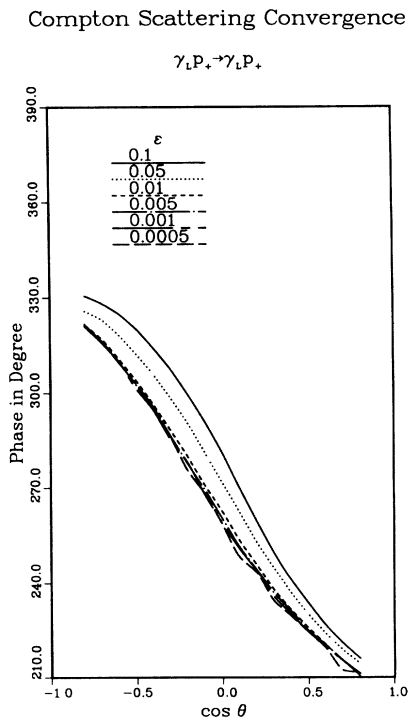

FIG. 3. Predictions for the phase of $\gamma_L p_+ \to \gamma_L p_+$, for various choices of ϵ.

III. $eN \to eN'\gamma$

As shown in Fig. 1, $e(k,h_e)N(p,h_N) \to e(k',h_e)N'(p',h_N)\gamma(q',\lambda')$ receives contributions from both virtual Compton and Bethe-Heitler scattering. Since the latter is well known experimentally, study of the angular dependence of $eN \to eN'\gamma$ is in principle a good method of investigating the phase structure of the virtual Compton process. We give below formulas for the Bethe-Heitler contribution to the $eN \to eN'\gamma$ helicity amplitudes, $B^{\lambda'}_{h_N h_e}$, in terms of the chirality-nonflip form factor of the nucleon, $F_1^N(q^2)$. We also give formulas for the virtual Compton contribution to $eN \to eN'\gamma$, denoted $A^{\lambda'}_{h_N h_e}$, in terms of the VC amplitudes, denoted $V^{\lambda\lambda'}_{h_N}$. Here h_e and h_N are the electron and nucleon helicities, and λ' and λ are the polarizations of the produced and virtual photons, respectively. A single helicity label for each fermion line is sufficient because in the leading-twist approximation used in this paper, initial and final helicities are the same. Likewise, we do not retain the contribution of the chirality-flip form factor, F_2^N.

All the formulas we give apply equally well whether N' is a nucleon or resonance such as Δ^+; in the latter case it is the transition form factor which enters the Bethe-Heitler amplitudes. For brevity we shall refer below to the final baryon as a nucleon. When we refer to an amplitude and include only some of its helicity or polarization labels, the statement is true for each of the possible choices for the other labels.

We select a reference frame such that the Compton scattering takes place in the center of momentum of the initial (virtual) photon and baryon, in the $\phi=0$ plane, with scattering angle θ, so that the initial and final proton and final photon momenta are

$$p = P(1,0,0,-1) ,$$

$$p' = Q'(1,-\sin\theta,0,-\cos\theta) ,$$

$$q' = Q'(1,\sin\theta,0,\cos\theta) .$$

Thus, when the reaction proceeds through virtual Compton scattering, the virtual photon has momentum

$$q = (\sqrt{P^2-Q^2},0,0,P) ,$$

i.e, $Q^2 = -q^2$. The initial and final electron momenta can be taken to be

$$k = K(1,\cos\phi\sin\alpha,\sin\phi\sin\alpha,\cos\alpha) ,$$

$$k' = K'(1,\cos\phi\sin\alpha',\sin\phi\sin\alpha',\cos\alpha') .$$

The nine parameters P, Q, Q', K, K', θ, ϕ, α, and α' are fixed in terms of the six independent invariants of the $eN \to eN'\gamma$ reaction by imposing the requirement that the virtual photon has $q_\perp = 0$, $q_z = P$, and $q_0 = k_0 - k_0' = p_0' + q_0' - p_0$. Thus we have

$$K\sin\alpha = K'\sin\alpha', \quad K\cos\alpha - K'\cos\alpha' = P ,$$

$$Q^2 = 4Q'(P-Q'), \quad s_{p'q'} = 2p'\cdot q' = 4Q'^2 ,$$

$$t_{pp'} = -2p\cdot p' = -2PQ'(1-\cos\theta) ,$$

$$s_{kp} = 2k\cdot p = 2KP(1+\cos\alpha) ,$$

$$t_{kk'} = -2k\cdot k' = -4KK'\cos^2(\alpha'-\alpha) ,$$

$$t_{kq'} = -2k\cdot q'$$
$$= -2KQ'(1-\sin\theta\cos\phi\sin\alpha - \cos\theta\cos\alpha) ,$$

$$s_{k'q'} = 2k'\cdot q'$$
$$= 2KQ'(1-\sin\theta\cos\phi\sin\alpha' - \cos\theta\cos\alpha') .$$

We reiterate that the leading-twist approximation which we make in our PQCD calculation is inherently inaccurate with respect to order-m^2/s corrections. Therefore differences between, e.g., the usual definition of $s_{kp} = (p+k)^2$ and the one given above in which m_p^2 and m_e^2 are dropped, lead to differences in the final prediction which are of the same order as the higher-twist corrections. If, in a practical calculation for a particular experiment, changing definitions of kinematic variables in this manner alters the prediction unacceptably, that means that the precision of the PQCD calculations is inadequate as well.

Real photons can take helicities L and R; a virtual photon can have polarization in the 0 (temporal) and 3 (longitudinal) directions as well. However the amplitudes for temporal and longitudinal polarizations are not independent: in our reference frame gauge invariance requires

$$\frac{V^3}{V^0} = \frac{s_{p'q'}-Q^2}{s_{p'q'}+Q^2} .$$

When we report VC amplitudes in the following it is therefore sufficient to give the combination $V^+ = (V^0 + V^3)/2$.

We give the positive-baryon-helicity amplitudes; amplitudes for negative baryon helicity are related by parity, so they are obtained by interchanging $R \leftrightarrow L$ and $+ \leftrightarrow -$. For instance, $B^R_{-+} = B^L_{+-}$, $V^{LR}_- = V^{RL}_+$, and $V^{+L}_- = V^{+R}_+$. The Bethe-Heitler contributions to $eN \to eN'\gamma$ are

$$B^R_{++} = c_\alpha(e^{-i\phi}s_{\alpha'}c - c_{\alpha'}s)$$
$$\times \frac{K'(e^{i\phi}s_{\alpha'}s + c_{\alpha'}c)(e^{-i\phi}s_{\alpha'}s + c_{\alpha'}c) + Q'}{s_{k'q'}}$$
$$+ (e^{-i\phi}s_{\alpha'}s + c_{\alpha'}c)(e^{i\phi}s_\alpha s + c_\alpha c)$$
$$\times \frac{Kc_\alpha(e^{-i\phi}s_\alpha c - c_\alpha s)}{t_{kq'}} , \tag{1}$$

$$B^L_{++} = c_\alpha(e^{-i\phi}s_{\alpha'}s + c_{\alpha'}c)$$
$$\times \frac{K'(e^{i\phi}s_{\alpha'}c - c_{\alpha'}s)(e^{-i\phi}s_{\alpha'}s + c_{\alpha'}c)}{s_{k'q'}}$$
$$+ (e^{-i\phi}s_{\alpha'}s + c_{\alpha'}c)(e^{i\phi}s_\alpha c - c_\alpha s)$$
$$\times \frac{Kc_\alpha(e^{-i\phi}s_\alpha s + c_\alpha c) - Q'c}{t_{kq'}} , \tag{2}$$

$$B^R_{+-}=(e^{-i\phi}s_{\alpha'}c-c_{\alpha'}s)(e^{i\phi}s_\alpha s+c_\alpha c)\times\frac{K'(e^{i\phi}s_{\alpha'}s+c_{\alpha'}c)c_{\alpha'}+Q'c}{s_{k'q'}}+c_{\alpha'}(e^{i\phi}s_\alpha s+c_\alpha c)\times\frac{K(e^{i\phi}s_\alpha c+c_\alpha c)(e^{-i\phi}s_\alpha c-c_\alpha s)}{t_{kq'}}, \quad (3)$$

$$B^L_{+-}=(e^{-i\phi}s_{\alpha'}s+c_{\alpha'}c)(e^{i\phi}s_\alpha s+c_\alpha c)\times\frac{K'(e^{i\phi}s_{\alpha'}c-c_{\alpha'}s)c_{\alpha'}}{s_{k'q'}}+c_{\alpha'}(e^{i\phi}s_\alpha c-c_\alpha s)\times\frac{K(e^{i\phi}s_\alpha c+c_\alpha c)(e^{-i\phi}s_\alpha s+c_\alpha c)-Q'}{t_{kq'}} \quad (4)$$

times the common factor

$$c_B=-e^3\frac{F_1(t_{pp'})}{t_{pp'}}2^4\sqrt{2KK'PQ'}\ .$$

We have used the abbreviations $c=\cos\theta/2$, $c_\alpha=\cos\alpha/2$, $c_{\alpha'}=\cos\alpha'/2$, $s=\sin\theta/2$, $s_\alpha=\sin\alpha/2$, $s_{\alpha'}=\sin\alpha'/2$.

The virtual Compton contributions to the $eN\to eN'\gamma$ amplitudes are

$$A^R_{+-}=c_{\alpha'}c_\alpha V^{-R}_{+}+s_{\alpha'}s_\alpha V^{+R}_{+}-e^{i\phi}c_\alpha s_{\alpha'}V^{LR}_{+}-e^{-i\phi}s_\alpha c_{\alpha'}V^{RR}_{+}\ , \quad (5)$$

$$A^R_{++}=c_{\alpha'}c_\alpha V^{-R}_{+}+s_{\alpha'}s_\alpha V^{+R}_{+}-e^{i\phi}s_\alpha c_{\alpha'}V^{RR}_{+}-e^{-i\phi}c_\alpha s_{\alpha'}V^{LR}_{+} \quad (6)$$

times the common factor $c_A=+2e\sqrt{2KK'}/Q^2$. Expressions for the A^L amplitudes are obtained from (5) and (6) by replacing the V^R's with V^L's. Similarly replacing V_+'s with V_-'s gives the A's on a negative-helicity baryon.

The expressions above for the Bethe-Heitler and VC contributions are most easily obtained using the method of Farrar and Neri.[6] To fix conventions, we give the unpolarized differential cross section for $eN\to eN\gamma$ in terms of the helicity amplitudes A and B:

$$d\sigma=\frac{1}{4}\sum_{\substack{h_e=\pm\\ h_N=\pm\\ \lambda'=R,L}}\frac{1}{2p_02k_0}(2\pi)^{-5}\int\delta^4(p+k-p'-q'-k')\times\frac{d^3k'}{2k'_0}\frac{d^3p'}{2p'_0}\frac{d^3q'}{2q'_0}\times|A^{\lambda'}_{h_Nh_e}+B^{\lambda'}_{h_Nh_e}|^2\ .$$

IV. RESULTS FOR THE HELICITY AMPLITUDES

In this section we present results of the calculations described in Sec. II for $\gamma^{(*)}N\to\gamma N'$, using the nucleon wave functions of Chernyak, Ogloblin, and Zhitinsky (COZ) (Ref. 7), Δ wave functions of Farrar, Zhang, Ogloblin, and Zhitnitsky (FZOZ) (Ref. 8), and $\alpha_s=0.3$. The perturbative QCD predictions for G^p_M and $\psi\to p\bar{p}$, using this value of α_s and wave function, are in good agreement with experiment.

Actually, rather than amplitudes, we give the contributions of individual helicity channels to the unpolarized Compton scattering differential cross sections,

$$\left[\frac{d\sigma}{dt}\right]_{LR}\equiv\frac{1}{16\pi s^2}(0.389\times10^6\ \text{nb GeV}^2)|V^{LR}_{+}|^2\ ,$$

where, as in the previous section, we let the nucleons have positive helicity and use V to denote Compton amplitudes, even when $q^2=0$. In separate figures, we give the phases of each helicity amplitude. The leading-twist energy dependence, s^{-6}, is automatically that predicted from dimensional arguments.[9,10] We computed the amplitudes at $\cos\theta=0,\pm0.2,\pm0.4,\pm0.6,\pm0.8$. Each point has some error from the numerical integration, but rather than fit to a smooth function, we elected to prepare the figures by simply connecting the calculated values by a smooth curve. Thus the waviness in the curves provides a measure of the uncertainty in the predictions. It does not reflect any physics.

Figures 4–15 show the "helicity cross sections" and phases for $\gamma p_+\to\gamma p_+$, for $Q^2/s=0.0$, 0.25, 0.5, 0.75, 1.0. The Q^2 dependence and phase structure is extremely complex and interesting. The magnitude of the dominant amplitude $\gamma_R p_+\to\gamma_R p_+$, denoted RR below, does not change greatly with increasing Q^2, except that it drops in the vicinity of $Q^2/s\sim0.25$, for scattering which is not in the backward hemisphere. However the LL am-

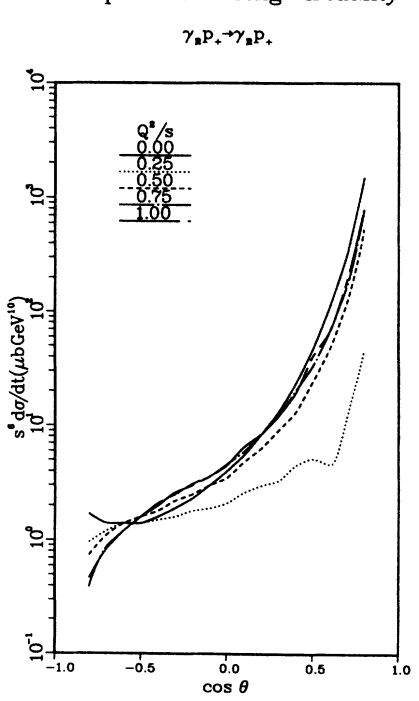

FIG. 4. $\gamma_R p_+\to\gamma_R p_+$ helicity cross section for several values of Q^2, using the COZ wave function and $\alpha_s=0.3$ throughout, except for Figs. 26 and 27.

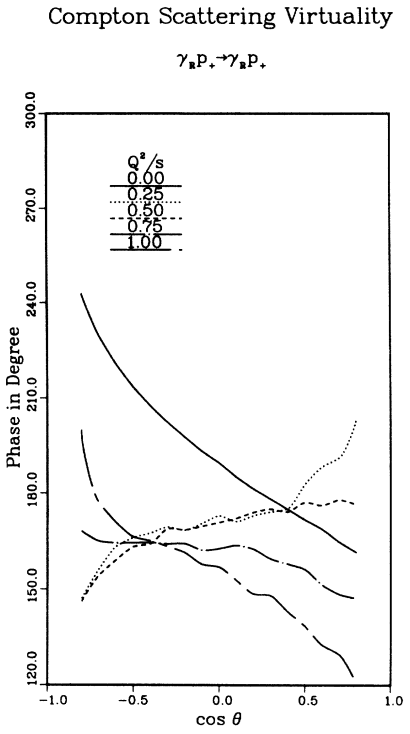

FIG. 5. Phase of the $\gamma_R p_+ \to \gamma_R p_+$ helicity amplitude for several values of Q^2.

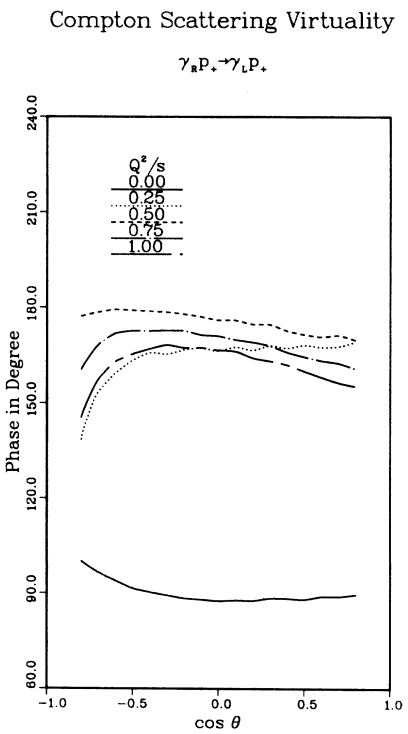

FIG. 7. Phase of the $\gamma_R p_+ \to \gamma_L p_+$ helicity amplitude for several values of Q^2.

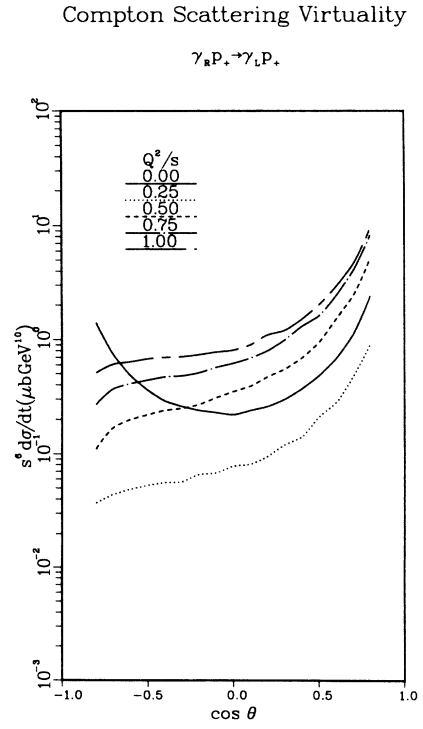

FIG. 6. $\gamma_R p_+ \to \gamma_L p_+$ helicity cross section for several values of Q^2.

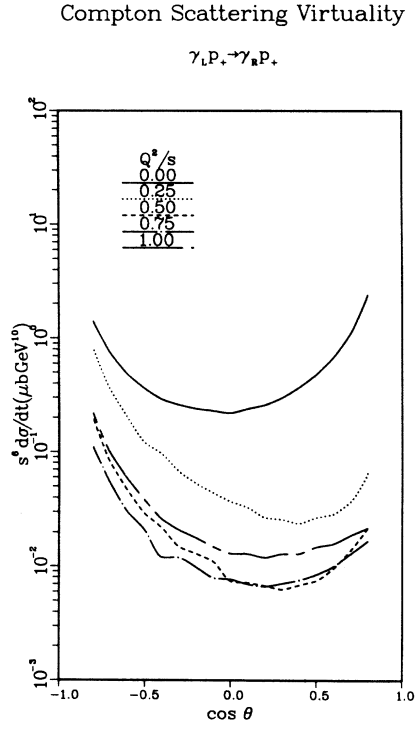

FIG. 8. $\gamma_L p_+ \to \gamma_R p_+$ helicity cross section for several values of Q^2.

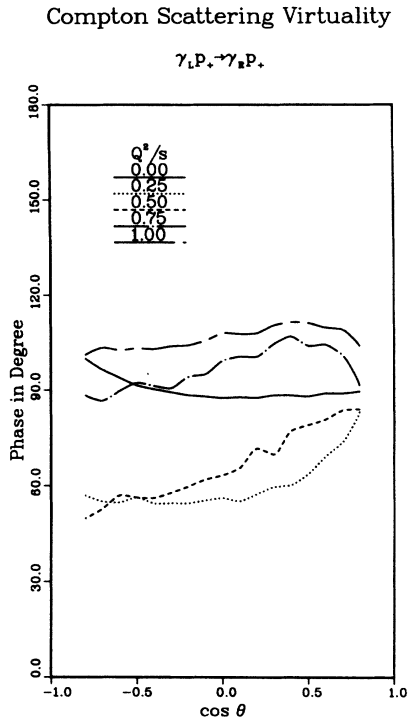

FIG. 9. Phase of the $\gamma_L p_+ \to \gamma_R p_+$ helicity amplitude for several values of Q^2.

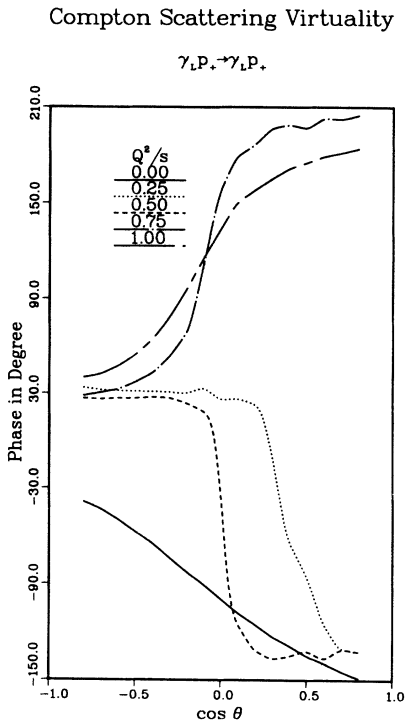

FIG. 11. Phase of the $\gamma_L p_+ \to \gamma_L p_+$ helicity amplitude for several values of Q^2.

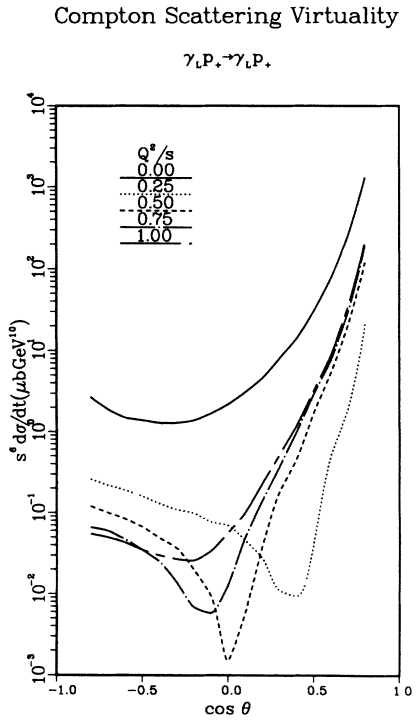

FIG. 10. $\gamma_L p_+ \to \gamma_L p_+$ helicity cross section for several values of Q^2.

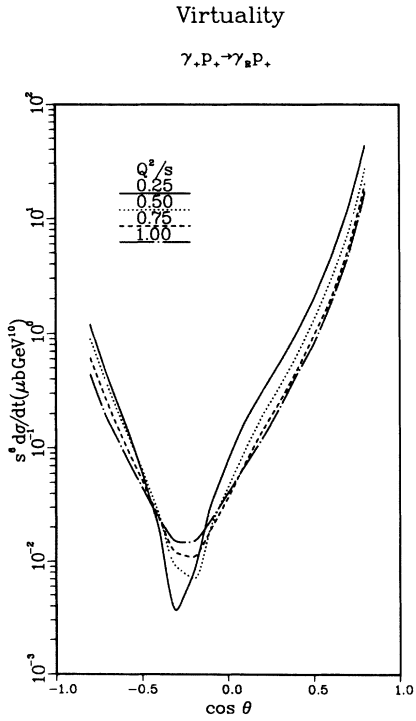

FIG. 12. $\gamma_+ p_+ \to \gamma_R p_+$ helicity cross section for several values of Q^2.

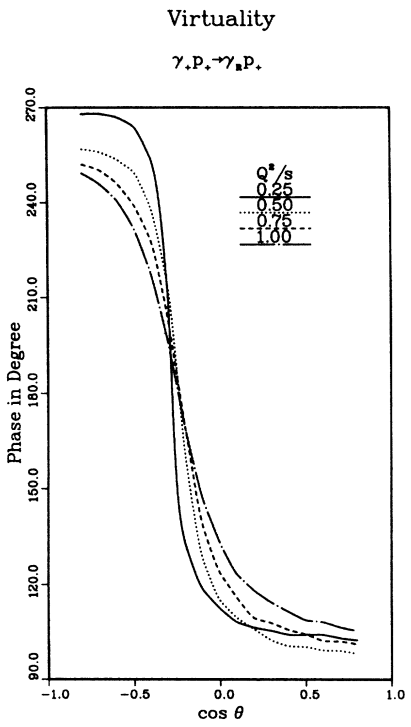

FIG. 13. Phase of the $\gamma_+ p_+ \to \gamma_R p_+$ helicity amplitude for several values of Q^2.

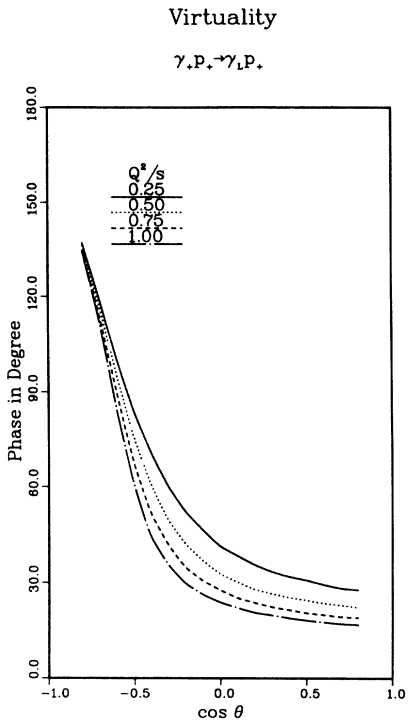

FIG. 15. Phase of the $\gamma_+ p_+ \to \gamma_L p_+$ helicity amplitude for several values of Q^2.

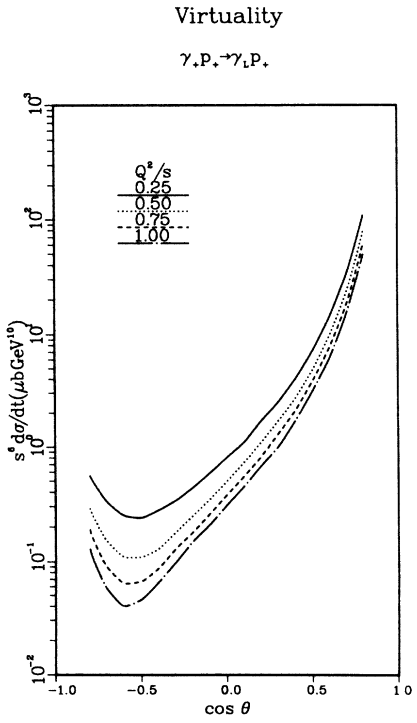

FIG. 14. $\gamma_+ p_+ \to \gamma_L p_+$ helicity cross section for several values of Q^2.

plitude has a dramatic dip at 90° for $Q^2 = s/2$ ($\cos\theta \approx 0.4$ for $Q^2 = s/4$). The RL amplitude grows with Q^2, but the LR amplitude falls. These four amplitudes show strong variation in the phase structure as a function of Q^2.

Both $+L$ and $+R$ grow with Q^2 as expected, but the latter has a strong dip for $\cos\theta \sim -\frac{1}{4}$. We calculated the amplitudes for $Q^2/s = 0.125$, to make sure there was no problem with the $q^2 \to 0$ limit, particularly for the LL amplitudes which show such a strong dip. Since the results fall between the $Q^2/s = 0$ and 0.25 curves, we do not include them in the figures for clarity.

If these features can be investigated in detail experimentally, it will be a very powerful test of our theoretical understanding of both perturbative QCD for exclusive Compton scattering and the accuracy of our wave functions, as will be elaborated below.

In Figs. 16–23 we see the real Compton predictions for other flavor channels, beginning with $\gamma p \to \gamma \Delta^+$ in Figs. 16 and 17. Here, the RR and LL cross sections are quite similar to one another, and in shape to $\gamma_R p \to \gamma_R p$, but almost an order of magnitude smaller. For $\gamma n \to \gamma n$ (Figs. 18 and 19) the RR and RL cross sections are similar in shape to their $\gamma p \to \gamma p$ counterparts, just a factor-of-3 smaller. On the other hand, LL has a quite different shape: it resembles more closely the virtual LL cross sections. The $\gamma n \to \gamma \Delta^0$ cross sections (Figs. 20 and 21) are very similar in shape to, but about an order of magnitude smaller than, $\gamma n \to \gamma n$, just as seen in their charge $+1$ counterparts. The small size of $\gamma \Delta^+ \to \gamma \Delta^+$ shown in

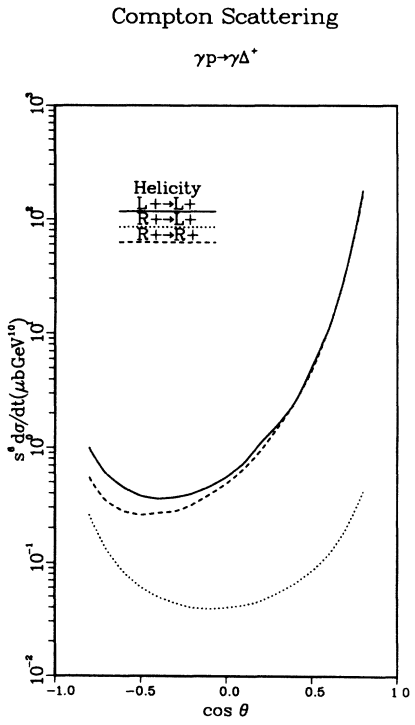

FIG. 16. $Q^2=0$ helicity cross sections for $\gamma p_+ \to \gamma \Delta^+_+$, using the FZOZ wave function for the Δ throughout.

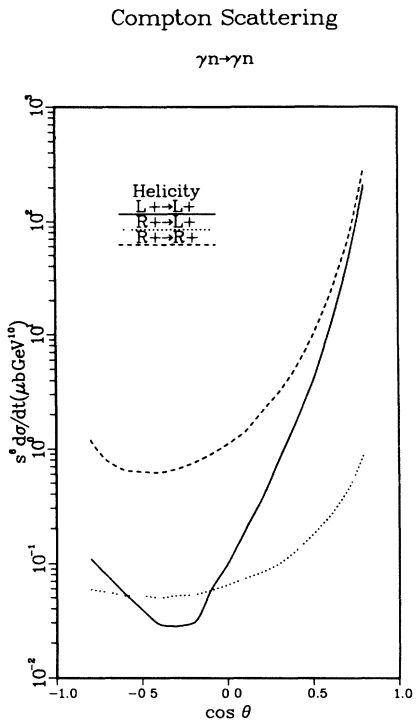

FIG. 18. $Q^2=0$ helicity cross sections for $\gamma n_+ \to \gamma n_+$.

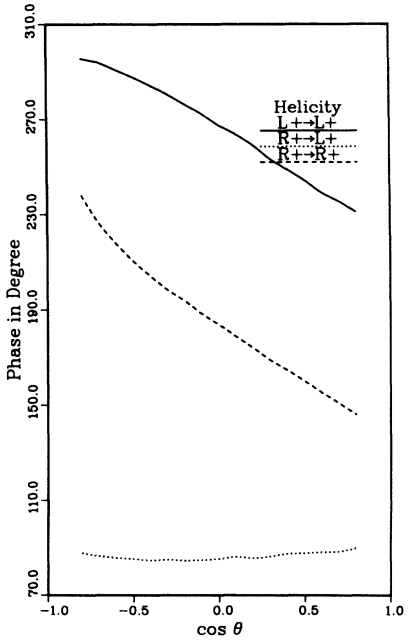

FIG. 17. Phases of the helicity amplitudes for $\gamma p_+ \to \gamma \Delta^+_+$ for $Q^2=0$.

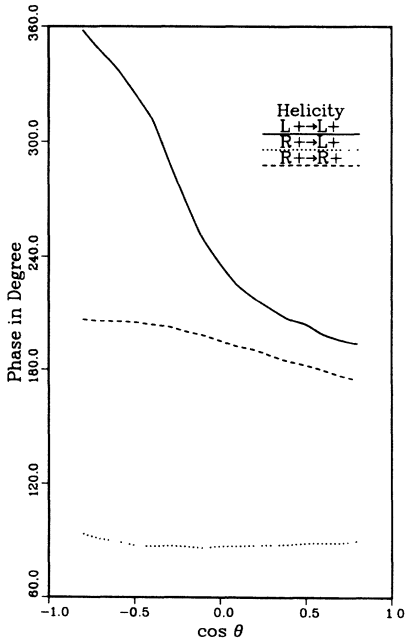

FIG. 19. Phases of the $Q^2=0$ helicity amplitudes for $\gamma n_+ \to \gamma n_+$.

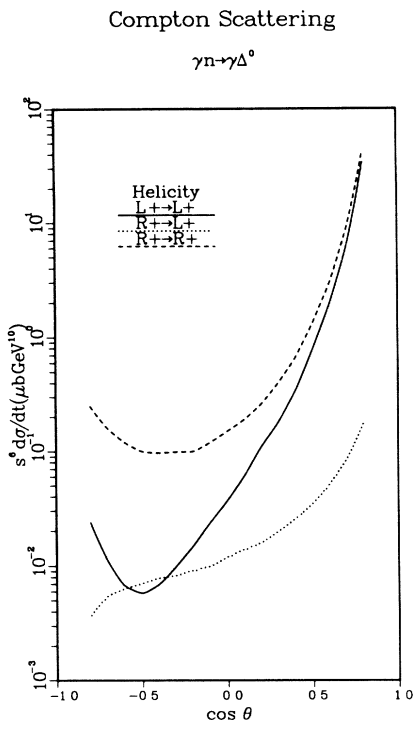

FIG. 20. $Q^2=0$ helicity cross sections for $\gamma n_+ \to \gamma \Delta^0_+$.

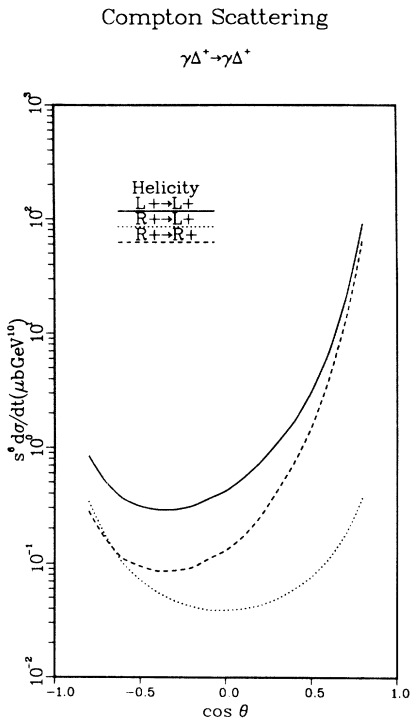

FIG. 22. $Q^2=0$ helicity cross sections for $\gamma \Delta^+_+ \to \gamma \Delta^+_+$.

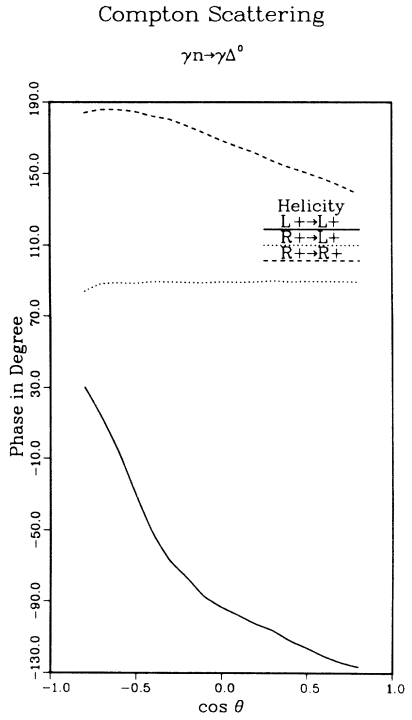

FIG. 21. Phases of the $Q^2=0$ helicity amplitudes for $\gamma n_+ \to \gamma \Delta^0_+$.

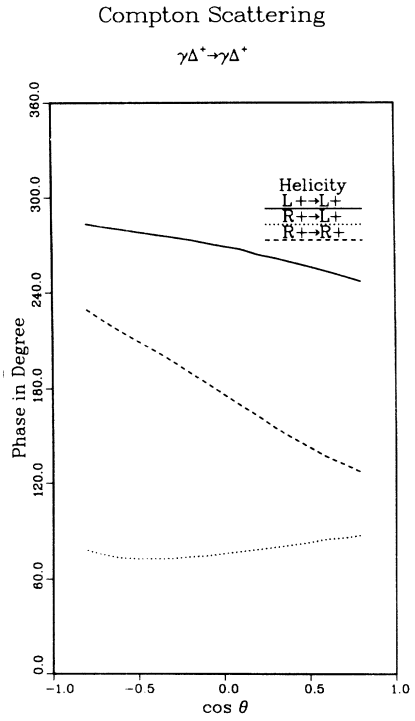

FIG. 23. Phases of the $Q^2=0$ helicity amplitudes for $\gamma \Delta^+_+ \to \gamma \Delta^+_+$.

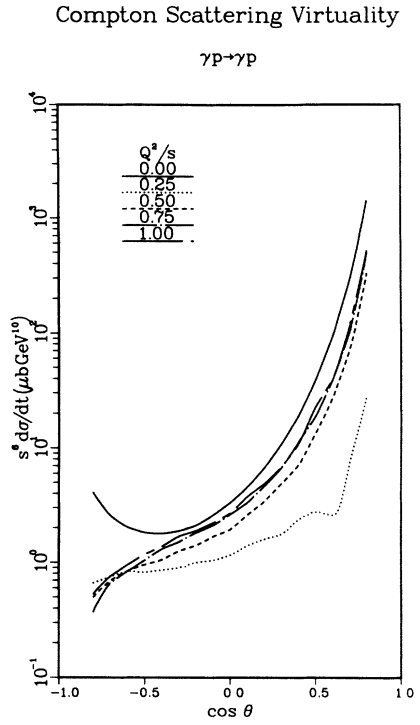

FIG. 24. Unpolarized cross section for $\gamma p \to \gamma p$ for $Q^2=0, s/4, s/2, 3s/4, s$.

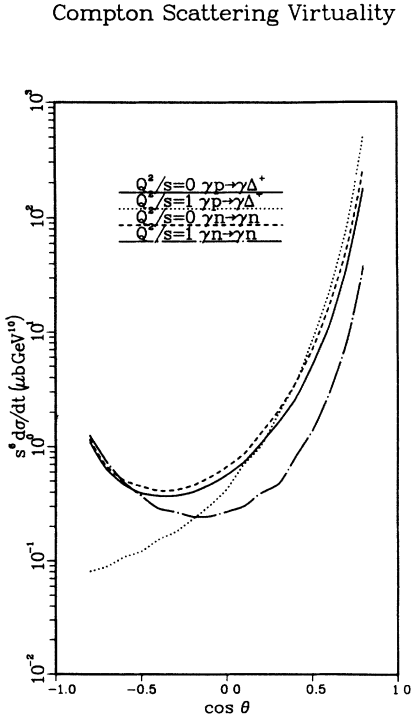

FIG. 25. Unpolarized cross sections for $\gamma p \to \gamma \Delta^+$ and $\gamma n \to \gamma n$ for $Q^2=0$ and s.

Figs. 22 and 23 reveals that the suppression of $\gamma p \to \gamma \Delta^+$ and $\gamma n \to \gamma \Delta^0$, compared to $\gamma p \to \gamma p$ and $\gamma p \to \gamma p$, is not just an issue of the orthogonality of the N and Δ wave functions. We will see in Sec. V that the form of the Δ wave function, which is qualitatively very similar to the asymptotic nucleon wave function, is responsible for the small size of these amplitudes. Evidently the gluon exchanges sufficiently "disrupt" the quark content that the final quarks do not "remember" their initial wave functions in detail.

Finally we give two figures for "unpolarized" cross sections, defined to be $\frac{1}{4}$ the sum over the L and R helicity cross sections even when the initial photon is virtual: since the amplitudes for temporal and longitudinal photon polarizations are negligible in comparison to the dominant amplitudes, how we treat them is unimportant. Figure 24 shows the Q^2 dependence of $\gamma p \to \gamma p$ and Fig. 25 shows it for $\gamma p \to \gamma \Delta^+$, and $\gamma n \to \gamma n$. It is remarkable that the $\gamma p \to \gamma p$ cross sections at large Q^2 are comparable to the $Q^2=0$ cross sections, with a minimum in the cross sections at $Q^2/s \sim \frac{1}{4}$. Also noteworthy is the prediction that the $\gamma n \to \gamma n$ and $\gamma p \to \gamma \Delta^+$ cross sections are extremely close in magnitude and angular dependence.

The reader must study these figures himself in order to fully appreciate the richness they reveal.

V. UNCERTAINTIES IN THE PREDICTIONS

How accurate are the predictions for Compton scattering given in the last section? The possible sources of uncertainty are the hadron wave function, the choice of α_s, higher-order corrections to the quark scattering amplitude, and nonleading-twist effects, a special case of which is the end-point sensitivity stressed by Isgur and Llewellyn Smith.[11]

The wave functions are uncertain for two reasons. First, they are q^2 dependent and their functional forms are only known[12] with certainty for infinite q^2; various model forms have been proposed and will be discussed in detail in a future publication. Second, the values of the moments of the wave function, obtained from QCD sum rules[7,13,8] and lattice QCD (Ref. 14) are uncertain. Restricting the wave function choices to ones which give a good accounting of G_M^p and $(\psi \to p\bar{p}/\psi \to \text{all})$ still leaves several candidate wave functions. We have therefore carried out the integrations for $\gamma p \to \gamma p$ using a number of wave functions. The results are summarized in Fig. 26. For each wave function, α_s has been set to the value which gives the best accounting of G_M^p; in each case it is quite close to 0.3. The form of the wave functions labeled COZ, KS (King-Sachrajda[13]), and CZ (Chernyak-Zhitnisky[15]) are the same (quadratic polynomials in the momentum fractions, multiplied by the asymptotic wave function). They differ only in that their moments correspond to the results of three different papers.[7,13,15] The CZ case is really only of historical interest, since that calculation was superseded by the COZ work. In principle, the KS and COZ calculations agree, so we do not understand why their moments are not in agreement. The difference, then, between curves COZ and KS—a factor

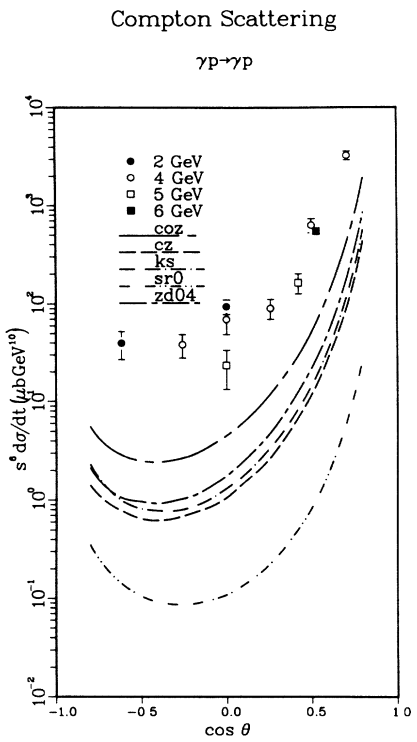

FIG. 26. Unpolarized $Q^2=0$ cross section for $\gamma p \to \gamma p$ for several different wave functions, compared to the data (Refs. 17–19).

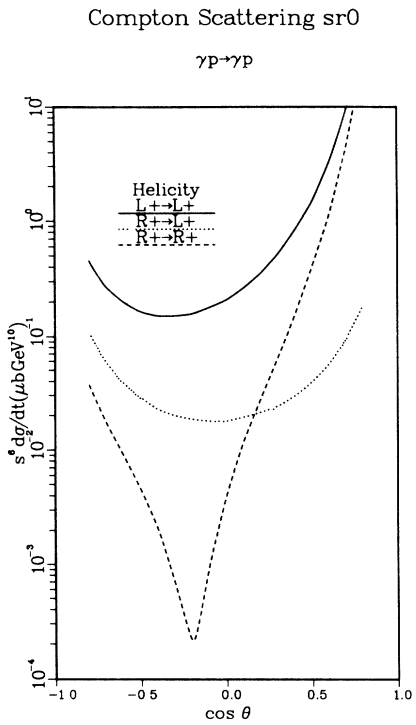

FIG. 27. $Q^2=0$ helicity cross sections for $\gamma p \to \gamma p$ with the asymptotic wave function.

of 2–3 in the unpolarized cross section—reflects the sensitivity of the predictions to the moment values.

The curve labeled ZD04 uses a wave function whose form is suggested by a light-cone quark model,[16] with its parameters constrained to yield the COZ moments. The difference between this curve and the COZ curve reflects the sensitivity to the form of the wave function: again, about a factor of 3.

The curve labeled sr0 is the prediction using the asymptotic wave function, normalized to the lowest sum-rule moment. It is not meant to be realistic for accessible energies, but is another indication of the sensitivity of the result to the form of the wave function, as well as its higher moments. It is also interesting because the actual Δ wave function is[8] practically asymptotic in its form, indicating that the small values of Compton cross sections involving Δ's result from the form of the Δ wave function, as mentioned in Sec. IV. Figure 27 shows the separate helicity cross sections for this asymptotic wave function, and its striking behavior at 90° in the RR channel. This phenomenon is probably similar in origin to the vanishing of G_M^p when the asymptotic wave function is used.

As for the other sources of uncertainty mentioned above, that due to the value of α_s is somewhat related to the question of the sensitivity of the result to the end-point region, i.e., to wave-function configurations in which one quark carries almost all the momentum. This is because sensitivity to the end-point region translates into sensitivity to the contributions of low-k^2 gluons and thus into sensitivity to the effective coupling at low k^2. On the other hand, since the value of α_s used in the Compton prediction gives G_M^p and $(\psi \to p\bar{p}/\psi \to \text{all})$ correctly for the wave function under consideration, there is little sensitivity to the uncertainty in α_s if the calculation is not sensitive to the end-point region. Since considerable controversy still surrounds the correct analysis of the end-point regions, we defer a quantitative discussion of this problem for a future publication and merely underline the need for caution in presuming that present experiments should necessarily conform to the predictions given here from perturbative QCD. It should be noted that end-point sensitivity, being a higher-twist effect, leads to an important deviation from the leading-twist scaling behavior.

As for higher-loop corrections, the canonical measure of their contribution is α/π in the amplitude, amounting to $\sim 20\%$ uncertainty in the cross section. Finally, higher-twist amplitudes can be estimated to be $\sim \lambda_{\rm QCD}^2/\langle k^2 \rangle$ times the leading-twist amplitude, where $\langle k^2 \rangle$ is the average virtuality of the gluons. Assuming in addition that $\langle k^2 \rangle/t$ for Compton is similar to that for the proton form factor, ~ 0.1, gives about a 10% uncertainty in the cross sections for 90° scattering at $s \sim 20$ GeV^2.

VI. COMPARISON WITH DATA

Figure 26 shows, along with the predictions of the various models for the proton wave functions, the largest

s,t,u data available for (real) Compton scattering on a proton target.[17–19] It can be seen that none of the models gives satisfactory agreement with the data as to absolute magnitude, nor is the s^{-6} scaling behavior accurately manifested at these low energies ($p_{\rm lab}=2-5$ GeV/c for 90° scattering). Nonetheless, the angular dependence of the predictions is in excellent agreement with observation and the s^{-6} scaling looks reasonable when the data is viewed as a whole, on a log plot. Since the magnitudes of the predictions are very sensitive to the detailed form of the wave function, but the angular dependence is not (see Fig. 26), an economical interpretation of the discrepancy between the predictions and the data is that the leading-twist approximation is valid for $p_{\rm lab}=5$ GeV/c at 90°, but we have not yet found the correct wave function for the proton. Alternatively, since even the form factor does not exhibit the asymptotic t^{-2} behavior until $t\sim-5$ GeV^2, and since there is a significant difference between $s^6 d\sigma/dt$ at 90° for various values of s, even at the highest energies, it is reasonable to regard this data as simply at too low an energy to be compared to asymptotic predictions.

VII. DISCUSSION

Our most interesting result is the discovery of the remarkable structure in many of the virtual Compton scattering amplitudes as Q^2/s and θ are varied. We investigated the origin of this structure at the level of the individual Feynman diagrams, and discovered the following.

(a) Diagrams in which both photons attach to a single quark line generally give substantially larger contributions than those in which they attach to different quark lines.

(b) In the kinematic regime exhibiting the dramatic structure, the full amplitude, which is the sum of all the ($\sim$100) Feynman diagrams, is much smaller than the magnitudes of the largest diagrams. That is, there is very substantial cancellation between the different diagrams.

(c) The dominant diagrams' contributions individually vary rather smoothly; the strong structure of the full amplitude arises from shifts in the delicate balance between diagrams.

This kind of collective behavior of many Feynman diagrams, while clearly a theoretical possibility, has generally been dismissed in the quest for finding the "dominant" mechanism for exclusive scattering. It has also been claimed that PQCD would necessarily give only smooth variation, and thus could not explain the dramatic structure seen in various spin observables in pp scattering, as a function of kinematical variables. Our results for virtual Compton scattering show that the previous discussion of these other issues has been too simplistic; much more work will be needed before any firm conclusions can be drawn.

Hopefully the results presented here will spur the theoretical community to improve the accuracy of the moments of the proton wave function, and to develop a sound theoretical basis for choosing a form for the wave function. Compton scattering deserves renewed experimental study. We have seen in this paper that QCD predicts a wealth of complicated and sometimes surprising behavior. Accurate data at larger momentum transfer will be most welcome.

ACKNOWLEDGMENTS

We are grateful for the cooperation of E. Maina who supplied us with his computer programs used in the calculations reported in Refs. 2 and 3 in order for us to track down the discrepancies between his results and those presented here. Thanks also go to Karl van Bibber and Charles Hyde-Wright for helpful discussions and suggestions. G.R.R. was supported in part by Grant No. NSF-PHY-88-18535. H.Z. was supported by Grant No. NSF-PHY-88-18535.

[1] G. R. Farrar, G. Sterman, and H. Zhang, Phys. Rev. Lett. **62**, 2229 (1989).
[2] E. Maina, Ph.D. thesis, Rutgers, 1985.
[3] G. R. Farrar and E. Maina, Phys. Lett. B **206**, 120 (1988).
[4] G. R. Farrar, E. Maina, and F. Neri, Nucl. Phys. **B259**, 702 (1985).
[5] J. Gunion, D. Miller, and K. Sparks, Phys. Rev. D **33**, 689 (1986).
[6] G. R. Farrar and F. Neri, Phys. Lett. **130B**, 109 (1983).
[7] V. Chernyak, A. Ogloblin, and I. Zhitnitsky, Report No. INP-134-1987, Novosibirsk, 1987 (unpublished).
[8] G. R. Farrar, H. Zhang, A. A. Ogloblin, and I. R. Zhitnitsky, Nucl. Phys. **B311**, 585 (1988).
[9] G. R. Farrar and S. J. Brodsky, Phys. Rev. Lett. **31**, 1153 (1973).
[10] G. R. Farrar and S. J. Brodsky, Phys. Rev. D **11**, 1309 (1975).
[11] N. Isgur and C. Llewellyn Smith, Phys. Lett. B **217**, 535 (1989).
[12] G. Lepage and S. Brodsky, Phys. Rev. D **22**, 2157 (1980).
[13] I. King and C. Sachrajda, Nucl. Phys. **B279**, 785 (1987).
[14] G. Martinelli and C. Sachrajda, Report No. CERN-TH.4637/87, 1987 (unpublished).
[15] V. Chernyak and A. Zhitnitsky, Phys. Rep. **112**, 173 (1984).
[16] Z. Dziembowski, Phys. Rev. D **37**, 2030 (1988).
[17] M. Deutsch *et al.*, Phys. Rev. D **8**, 3828 (1973).
[18] M. A. Shupe *et al.*, Phys. Rev. D **19**, 1921 (1979).
[19] J. Duda *et al.*, Z. Phys. C **17**, 319 (1983).